

Article

Open Access



Synergistic effect study of g-C₃N₄ composites for high-performance triboelectric nanogenerators

Yana Xiao, Jian Lu, Bingang Xu*

Nanotechnology Center, School of Fashion and Textiles, The Hong Kong Polytechnic University, Hong Kong 999077, China.

*Correspondence to: Prof. Bingang Xu, Nanotechnology Center, School of Fashion and Textiles, The Hong Kong Polytechnic University, 11 Yuk Choi Road, Hung Hom, Kowloon, Hong Kong 999077, China. E-mail: tcxubg@polyu.edu.hk

How to cite this article: Xiao, Y.; Lu, J.; Xu, B. Synergistic effect study of g-C₃N₄ composites for high-performance triboelectric nanogenerators. *Energy Mater.* 2025, 5, 500057. <https://dx.doi.org/10.20517/energymater.2024.155>

Received: 2 Sep 2024 **First Decision:** 4 Nov 2024 **Revised:** 18 Nov 2024 **Accepted:** 9 Dec 2024 **Published:** 26 Feb 2025

Academic Editors: Lei Wang, Yuping Wu **Copy Editor:** Ping Zhang **Production Editor:** Ping Zhang

Abstract

The energy harvesting crisis has caused great necessity for new energy technologies, among which triboelectric nanogenerators (TENGs) garnered global attention. Based on our previous research on a novel 2D material graphitic carbon nitride (g-C₃N₄), this work explores the influence of g-C₃N₄ hybrid dopants with Polydimethylsiloxane (PDMS) on the performance enhancement of TENGs. More specifically, systematic experiments with different ratios of hybrid dopants were conducted, including Ag nanowires with g-C₃N₄, carbon nanotubes with g-C₃N₄, and MXene with g-C₃N₄. The systematic and optimization studies showed that carbon nanotube/g-C₃N₄ at the optimal ratio of 1:1 in PDMS composite presented an open circuit voltage (*V*_{oc}) at 122 V, a short circuit current (*I*_{sc}) at 5.8 μA, and a charge transfer (*Q*_{sc}) at 105 nC, while Ag/g-C₃N₄ at the ratio of 3:1 with 1 wt % in PDMS composite presented the best performance with *V*_{oc} of 92 V, *I*_{sc} of 4.6 μA, *Q*_{sc} of 49 nC, and power density of 1.45 W/m². The fabricated hybrid dopant/PDMS TENG was utilized for versatile applications in biomechanical energy harvesting and self-powered human-motion detecting. In addition, we designed a dish and an insole with multiple TENGs for pressure sensing and multichannel data acquisition applications.

Keywords: Triboelectric nanogenerator, hybrid dopants, graphitic carbon nitride, multichannel sensor

INTRODUCTION

The world is in constant pursuit of sustainable energy sources. Sustainable and net carbon emission power sources are playing a thriving role due to booming energy consumption in the new era^[1]. Promising



© The Author(s) 2025. **Open Access** This article is licensed under a Creative Commons Attribution 4.0 International License (<https://creativecommons.org/licenses/by/4.0/>), which permits unrestricted use, sharing, adaptation, distribution and reproduction in any medium or format, for any purpose, even commercially, as long as you give appropriate credit to the original author(s) and the source, provide a link to the Creative Commons license, and indicate if changes were made.



alternatives for powering wearable devices such as piezoelectric nanogenerators (PENGs), pyroelectric nanogenerators, moisture electric generators, triboelectric nanogenerators (TENGs)^[2], tribovoltaic nanogenerators (TVNGs) have presented high output performance, environmental friendliness, self-power capability for various applications, *etc.* Among these, TENGs are a technology that holds tremendous promise including low cost^[3], simple fabrication, high efficiency, versatile structural designs^[4], diversity of material selection, sustainability^[5], *etc.*

A TENG is a device that harnesses the triboelectric effect, a phenomenon where a material gains or loses electrons when it contacts a different material, generating a charge difference. By leveraging this effect, TENGs can convert mechanical energy from everyday activities such as walking, running, typing, or natural movement including wind and tide, into electrical energy^[6]. This technology is incredibly innovative, highly reliable, and long-lasting, making it ideal for use in wearable devices^[7]. The potential applications of TENGs are from powering electronic devices to capturing energy from humans or the environment. Hence, extensive effort has been made to design and fabricate self-powered sensors, sustainable energy sources, and wearable intelligent systems through the approach of nanogenerators.

Polymers usually obtain low dielectric constant and hence possess low capacitance, and low charge abstaining capacity for being addressed as TENGs, especially during application with other electronic devices. Polydimethylsiloxane (PDMS) is a bio-friendly, non-toxic, flexible, highly durable, translucent, low-cost, and highly electronegative material with various excellent properties, making it ideal for wearable devices and sensors in the era of the Internet of Things. Because it can convert from liquid gel to elastic solid at room or high temperature, PDMS^[8] is well-suited for blending with nanoparticles to form composites. From the perspective of large-scale production, the most realistic option is the introduction of high-dielectric materials into common dielectric to significantly enhance permittivity and electrical performance^[9].

In the context of TENGs, doping is used to enhance the triboelectric properties to generate electrical energy through the triboelectric effect of PDMS. The simplest option is the introduction of high-dielectric ceramic materials such as BaTiO₃ or SrTiO₃^[10] into the polymer matrix which inherently possesses a comparatively low dielectric constant. Also, some other dopants such as MXene, carbon nanotubes (CNTs)^[11], metal nanoparticles^[12], and two-dimensional (2D) materials^[13] have been widely adopted and researched. The goal of doping PDMS in TENGs is to increase its ability to generate electrical energy and improve its other functions such as stability, durability, flexibility, transparency, *etc.*, thereby enhancing its overall performance. By optimizing the doping process and concentration ratio, significant improvements in the efficiency and output of TENGs can be achieved, making them a more practical and feasible solution for energy application^[14].

Two-dimensional materials are attractive for fabricating flexible and lightweight or multifunctional TENG devices. The triboelectric properties of graphene or graphene oxide and different transition metal dichalcogenides (TMDs) have been studied previously^[15]. As a novel 2D material-graphitic phase carbon nitride which has sp² hybridized carbon nitrogen bonding similar to graphene, graphitic carbon nitride (g-C₃N₄) possesses advantages such as stability, wide bandgap, excellent thermal or chemical stability, and sensitivity to visible light. In our previous research on this material^[16], simple addition of g-C₃N₄ in PDMS could increase the output of TENGs. To our knowledge, the current approach on the effect of different and systematic combinations or g-C₃N₄ hybrid dopants with PDMS had not been studied or reported.

Based on our previous work of novel 2D material g-C₃N₄, we further studied different g-C₃N₄ composites with various dopants innovatively, such as CNTs, silver metal nanoparticles, MXene, and silver oxide (AgO), at different concentrations and ratios to optimize the electrical output of hybrid dopants and originally summarize the generality with varying combinations of dopants. In this research, we individually co-doped g-C₃N₄ with four different substances, focused on the characterization of Ag/g-C₃N₄ PDMS composite and optimized electrical performance at proper ratios for Ag/g-C₃N₄ PDMS TENG and CNT/g-C₃N₄ PDMS TENG specifically. The optimal ratio under different concentrations was identified and utilized for application. The combination of Ag nanoparticles and g-C₃N₄ showed greater enhancement than either single dopant, and the optimum output was achieved at a Ag:g-C₃N₄ ratio of 3:1 with open circuit voltage (*V_{oc}*) of 92 V, short circuit current (*I_{sc}*) of 4.6 μA, charge transfer (*Q_{sc}*) of 49 nC, which was four times higher than the performance of single dopants, and maximum power density achieved 1.45 W/m² under the resistance of 20 MΩ, at 100 N force/3 Hz frequency. Based on this TENG with hybrid dopants, a self-powered multifunctional harvester was fabricated, which could be attached or adhered to different parts of the human body for biomechanical energy harvesting and human motion detectors with versatile applications. When connected to multichannel acquisition and signal processing devices, we designed a novel disc device that detects pressure at different locations and an insole that tracks the center of gravity and gait to correct the walking posture. The easy fabrication and enhanced performance of TENGs with hybrid dopants had shown their prospect for industrialization.

RESULTS AND DISCUSSION

Fabrication and characterization

Figure 1A shows the schematic fabrication of TENGs incorporating hybrid dopants. Taking Ag/g-C₃N₄ PDMS as an example, after adding both silver and g-C₃N₄ nanoparticles into a PDMS solution, the molecular structure manifests as 2D framework, wherein each hexagonal unit of the g-C₃N₄ lattice encapsulates a single silver atom, facilitating synergistic interaction with increased conductivity, electron mobility, and more *Q_{sc}*^[17]. Then, the hybrid dopant PDMS composite was prepared using the blade-coating method, as illustrated in Figure 1B. The dopants included g-C₃N₄ powders combined with one of the following materials: Ag nanoparticles, MXene powders, nickel-coated CNTs, multiwall CNTs, or AgO, at different weight ratios. Figure 1C demonstrated the architecture of basic contact-separation mode TENGs, where the copper-nickel conductive fabric (CNF) acted as both positive dielectric and electrode, along with hybrid dopant/PDMS composite as negative dielectric, and the two dissimilar dielectric films were positioned facing with each other.

As CNTs were commonly used and had similar components with g-C₃N₄, we focused on the characterization of Ag/g-C₃N₄ PDMS composite. The X-ray diffraction analysis (XRD) of g-C₃N₄ powder was executed, as shown in Figure 1D, where a significant peak at 28° is indexed to crystalline phase g-C₃N₄. Surface functional groups were investigated by Fourier transform infrared spectroscopy (FTIR) where PDMS composite with different ratios of silver nanoparticles and g-C₃N₄ powders showed a similar pattern, as shown in Figure 1E, mainly showing the peaks of PDMS functional groups. Typical peaks of Ag nanoparticles at 2,921 cm⁻¹ and 1,029 cm⁻¹ were marked in the FTIR pattern. Typical peaks of PDMS included ~3,000 cm⁻¹ of CH₃, ~1,250 cm⁻¹ of Si-CH₃, ~1,000 cm⁻¹ for Si-O-Si, and ~750 cm⁻¹ of Si-CH₃. Generally, g-C₃N₄ showed a sharp absorption at ~807 cm⁻¹ where we could identify a peak around 800-850 cm⁻¹ in the FTIR pattern for all three composites with small drift.

The Raman spectrum of g-C₃N₄ typically displayed a peak at around 800-900 cm⁻¹ which was attributed to the in-plane stretching vibration of the carbon-nitrogen bonds, and another peak at around 1,300-1,400 cm⁻¹ which was related to the out-of-plane bending mode of the nitrogen atoms^[18]. Additionally, there might be

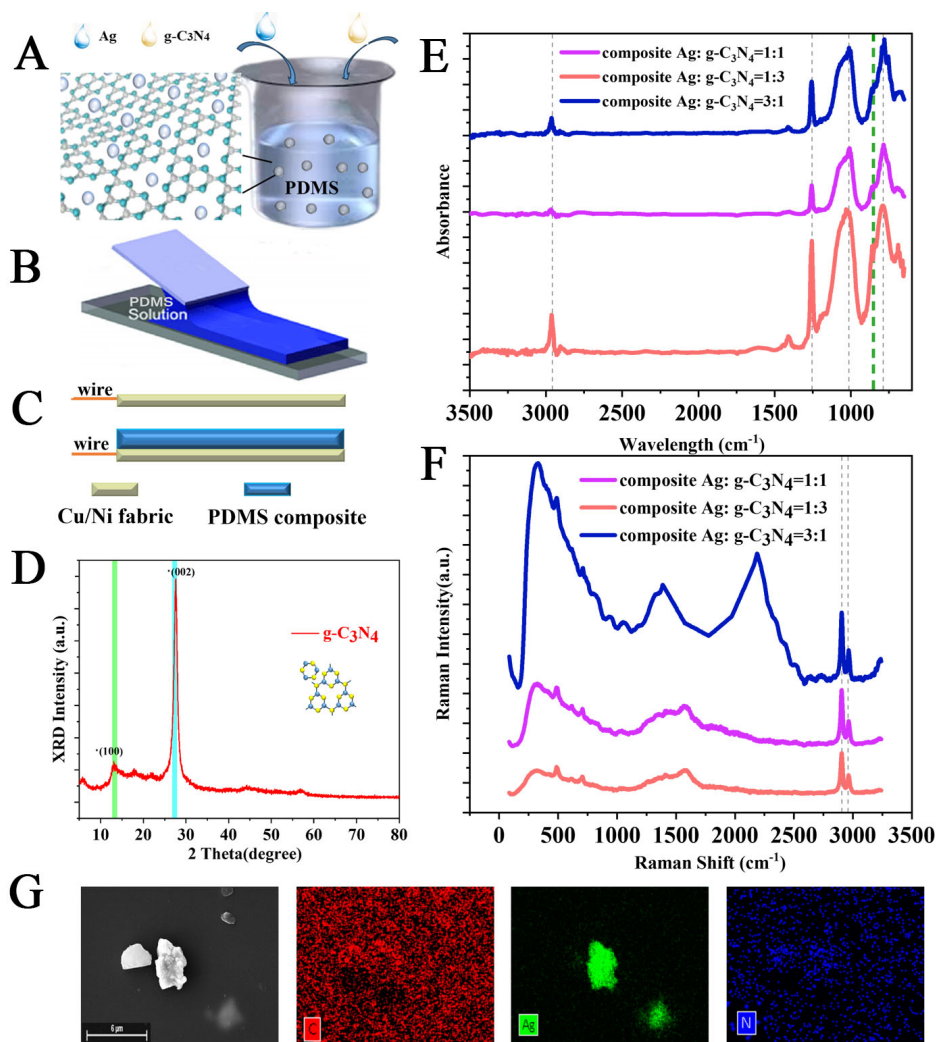


Figure 1. Illustration of fabrication of TENGs with hybrid dopants (taking dopants silver nanoparticle and $g\text{-C}_3\text{N}_4$ powder as an example). (A) Mixing of PDMS, silver nanoparticles, and $g\text{-C}_3\text{N}_4$ powders; (B) Blade coating of the mixture; (C) Structure of TENG; (D) XRD pattern of $g\text{-C}_3\text{N}_4$ powder; (E) FTIR spectra for PDMS composites with different ratios of Ag/ $g\text{-C}_3\text{N}_4$; (F) Raman spectra of a sample with 1 wt. % Ag/ $g\text{-C}_3\text{N}_4$ dopant at different proportions in PDMS composite; (G) SEM of Ag/ $g\text{-C}_3\text{N}_4$ PDMS composite and EDS mapping of elements. TENGs: Triboelectric nanogenerators; PDMS: polydimethylsiloxane; FTIR: fourier transform infrared spectroscopy; EDS: energy dispersive X-ray spectrometry; XRD: X-ray powder diffraction; SEM: scanning electron microscopy.

peaks at higher frequencies (above $1,600\text{ cm}^{-1}$) associated with the stretching modes of the carbon atoms in this material^[19]. The Raman spectrum of Ag typically showed several peaks corresponding to different vibrational modes of the Ag atoms or molecules in the sample, which could be divided into two categories. The first one was related to the translational and rotational vibrations of the Ag atoms, which were usually observed in the low-frequency region below 400 cm^{-1} . The second category corresponded to the vibrational modes of the molecules or clusters^[20], and typically appeared in the high-frequency region above 400 cm^{-1} . The most prominent peak in the Raman spectrum of Ag was typically associated with the longitudinal optical phonon mode (LO) at around 400 cm^{-1} ^[21]. It could be seen from Figure 1F that with the rise of Ag concentration, the band in the Raman spectrum had increased significantly. Other notable peaks in the Raman spectrum of Ag included the transverse optical phonon mode (TO) at around 430 cm^{-1} , the surface-enhanced Raman scattering (SERS) peak at around $1,600\text{ cm}^{-1}$, and the surface plasmon resonance (SPR) peak at around 380 nm in the ultraviolet-visible (UV-Vis) region^[22]. PDMS had one significant big

peak around $2,900\text{ cm}^{-1}$ and one small peak around 500 cm^{-1} ^[19]. The exact position and intensity of these peaks could depend on the specific synthesis method and composition. The position and intensity of these peaks provide information about the chemical composition, crystal structure, and bonding properties of the material. Scanning electron microscopy (SEM) and elemental mapping [energy dispersive X-ray spectrometry (EDS)] of Ag/g-C₃N₄ PDMS composite were also employed to display the distribution of certain dopants, as shown in [Figure 1G](#), which demonstrated the existence of silver, carbon and nitrogen elements.

The X-ray Photoelectron Spectroscopy (XPS) analysis [[Supplementary Figure 1](#)] was also conducted to observe constituent elements of Ag/g-C₃N₄ PDMS composite. From XPS spectra, apart from the constituent C and N elements, the presence of Ag could also be observed in the spectrum of the Ag/g-C₃N₄ PDMS composite^[23]. Because of the low concentration of doping, the N and Ag peaks were not significant. The existence of Ag nanoparticles and g-C₃N₄ nanosheets in PDMS might lead to a strong interaction between two materials due to the intimate attachment of the two materials, and N could donate the lone pair of electrons to the outermost orbital of Ag.

Mechanism

The schematic diagrams manifested the detailed working principle of a triboelectric device using the hybrid doped PDMS composite film as negative and CNF as positive triboelectric materials, respectively. From the first stage [[Figure 2AI](#)] where there was no electron transfer and electrode potential, the applied impact force [[Figure 2AII](#)] separated the two dielectrics, and then electrification induced the corresponding charges, which caused the charges to transfer from one electrode to another to balance the increased electric potential from decreasing capacity [[Figure 2AIII](#)]. While approaching, the charges returned from the positive to the negative electrode for the increasing capacity and form an opposite voltage and displacement current [[Figure 2AIV](#)]. The process of repeated contact and separation thus generated continuous alternating current (AC). The electric potential distribution was also simulated using COMSOL software to show the electricity-generating process, as shown in [Figure 2B](#). [Figure 2C](#) demonstrated a rectifier as an electronic device that converted AC into direct current (DC) with consistent polarity using one or more P-N junction diodes or bridge rectifiers^[24]. [Figure 2D](#) demonstrated a single alternate current pulse for one contact separation circle, where plus and minus peaks occurred while pressing and releasing and the repeated back-and-forth process acquired continuous voltage pulses and AC. [Figure 2E](#) illustrated the schematic structure of the PDMS composite TENG for output voltage (V), which is defined as^[25]:

$$V = \frac{(\sigma - \Delta\sigma) \cdot d_{gap}}{\epsilon_0} - \frac{\Delta\sigma \cdot d_{dopant / PDMS}}{\epsilon_0 \cdot \epsilon_{dopant / PDMS}} \quad (1)$$

where σ is the triboelectric charge density on the dopant/PDMS surface, $\Delta\sigma$ is the charge density transferred between electrodes, ϵ_0 is the vacuum permittivity, and $\epsilon_{dopant/PDMS}$ denotes the relative permittivity of the dopant/PDMS composite, d_{gap} stands for the inter-layer spacing, and $d_{dopant/PDMS}$ is the thickness of dopant/PDMS film. During open circuit conditions, the Q_{sc} is zero, indicating that V_{oc} is maximum when the gap reaches maximum and V_{oc} has no explicit dependency on the properties of triboelectric layers; however, σ surface charge density is related to the dielectric constant of the triboelectric material^[26].

Electrical output

To evaluate the triboelectric performance, the hybrid dopant/PDMS film was adhered to CNF to form the negative part, and the positive part was only CNF acting as both triboelectric material and electrode, which was then contacted and separated under an impact force of 100 N at a frequency of 3 Hz with an effective area of 4 cm². The CNF electrodes were connected through copper wire and then to the electrometer to measure and collect signals of V_{oc} , I_{sc} and Q_{sc} . Different ratios of Ag/g-C₃N₄ PDMS TENG and

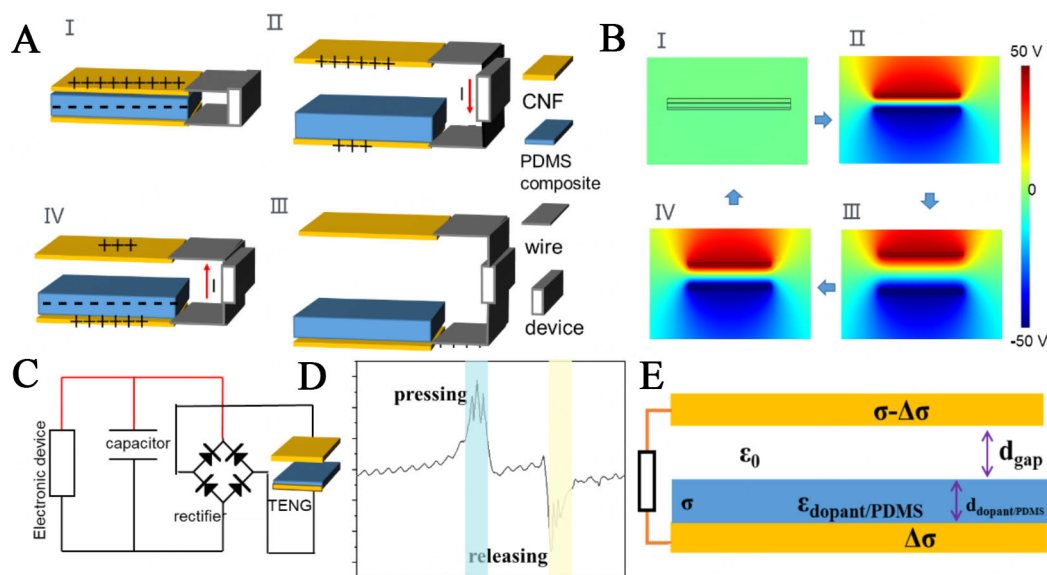


Figure 2. (A) (I-IV) Schematic diagrams of the working principle of contact and separation mode TENG; (B) Simulation results of electrical potential distribution by COMSOL Multiphysics software; (C) Equivalent circuit of a self-powered system TENG, capacitor, another device, and rectifier changing AC to DC; (D) Two opposite electric peaks during a single circle of contact and separation; (E) Schematic structure of dopant/PDMS TENG. TENGs: Triboelectric nanogenerators; AC: alternating current; DC: direct current; PDMS: polydimethylsiloxane.

CNT/g-C₃N₄ PDMS TENG were systematically prepared and evaluated, as shown in [Figure 3](#). [Supplementary Figure 2](#) displayed additional dopants we have experimented with g-C₃N₄, including nickel-coated CNTs [[Supplementary Figure 2A-C](#)], multiwall CNTs [[Supplementary Figure 2D-F](#)], three concentrations of MXene/g-C₃N₄ PDMS TENG [[Supplementary Figure 2G-I](#)], and g-C₃N₄ PDMS with and without AgO [[Supplementary Figure 2J-L](#)].

Based on our preliminary experimental results, the triboelectric performance increased significantly from dopant concentration 5 wt. % to 5 wt. %, so we selected the total doping content at 1 wt. % for practicality and comparability, which was each sample containing 9-gram elastomer, 1-gram curing agent, and 0.1-gram dopants in total.

The group of CNT and g-C₃N₄ dopants was composed of a different ratio for each sample, which were 0.1 g CNT, 0.075 g CNT+0.025 g g-C₃N₄ (3:1), 0.05 g CNT+0.05 g g-C₃N₄ (1:1), 0.025 g CNT+0.075 g g-C₃N₄ (1:3), and 0.1 g g-C₃N₄, respectively, with electric performance V_{oc} shown in [Figure 3A](#), I_{sc} in [Figure 3B](#), and Q_{sc} in [Figure 3C](#). The TENGs with hybrid dopants showed higher values of three parameters - V_{oc} , I_{sc} , and Q_{sc} - compared to those with a single dopant, either pure CNT or g-C₃N₄. The optimum concentration ratio to achieve the best electric performance was CNT: g-C₃N₄ = 0.05:0.05 (1:1), resulting in approximately 122 V for peak-peak V_{oc} , 5.8 μA for I_{sc} , and 105 nC for Q_{sc} . Conductive dopants could compete for a dual capacitive effect causing different performances with concentration and ratio changes^[27], which could be explained by the percolation theory. Once the CNT concentration exceeded the percolation threshold concentration (P_c), conductive paths would be formed due to the direct contact of the CNT dopants and the quantum tunnel effect^[28]. The triboelectric charge would be neutralized, thus decreasing the surface charge density^[29].

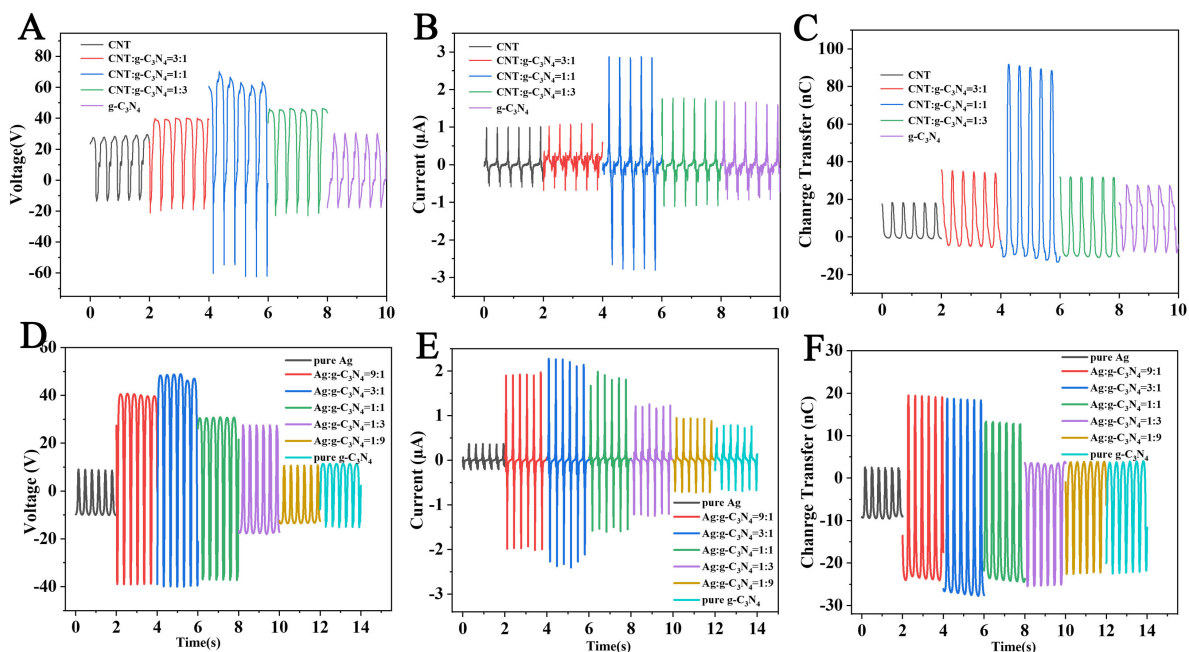


Figure 3. Electric performance of TENGs with hybrid dopants. (A) Open circuit voltage; (B) Short circuit current; and (C) Charge transfer of TENG with different ratios of carbon nanotube and $g\text{-C}_3\text{N}_4$ at a total weight proportion of 1 wt. %; (D) Open circuit voltage; (E) Short circuit current; and (F) Charge transfer of TENG with different ratios of Ag nanoparticles and $g\text{-C}_3\text{N}_4$ at a total weight proportion of 1 wt. %. TENGs: Triboelectric nanogenerators.

For another group of dopants Ag and $g\text{-C}_3\text{N}_4$, the dopant weight proportions were 0.1 g Ag, 0.09 g Ag+0.01 g $g\text{-C}_3\text{N}_4$ (9:1), 0.075 g Ag+0.025 g $g\text{-C}_3\text{N}_4$ (3:1), 0.05 g Ag+0.05 g $g\text{-C}_3\text{N}_4$ (1:1), 0.025 g Ag+0.075 g $g\text{-C}_3\text{N}_4$ (1:3), 0.01 g Ag+0.09 g $g\text{-C}_3\text{N}_4$ (1:9), 0.1 g $g\text{-C}_3\text{N}_4$, each for 10 g PDMS mixture, respectively. The optimum concentration ratio of Ag: $g\text{-C}_3\text{N}_4$ was 0.075:0.025 (3:1), resulting in a peak-to-peak V_{oc} of 92 V [Figure 3D], I_{sc} of 4.6 μA [Figure 3E], and Q_{sc} of 49 nC [Figure 3F], which was more than four times higher than that of either pure Ag or pure $g\text{-C}_3\text{N}_4$, approximately. When Ag nanoparticles and $g\text{-C}_3\text{N}_4$ powders were co-doped into PDMS, the doping ratio influenced the permittivity, potential difference, and triboelectric charge. However, an excessive amount of filler might lead to leakage current through the conduction path through the capacitive effect^[50]. Therefore, a suitable doping ratio was necessary to achieve optimal TENG performance.

Influence of external factors

The performance of TENGs can be influenced by frequency or external force, so we have evaluated the Ag/ $g\text{-C}_3\text{N}_4$ PDMS TENG at the optimum concentration ratio of 3:1, at different frequencies of 1 Hz, 2 Hz, 3 Hz, 4 Hz, 5 Hz and 6 Hz under a fixed external force of 100 N, and different external forces of 10 N, 50 N, 100 N, and 200 N under a fixed frequency of 2 Hz, respectively. When the frequency increased gradually from 1 Hz to 6 Hz, the performance did not change very much around 80 V for V_{oc} and about 25 nC for Q_{sc} but went up significantly from 2.2 μA to 6.8 μA for I_{sc} [Figure 4A-C]. As the external force rose progressively from 10 N to 200 N, the V_{oc} grew from 40 V to 130 V [Figure 4D]. Meanwhile, the I_{sc} climbed gradually from 2.0 μA to 10.2 μA [Figure 4E] and the Q_{sc} increased from approximately 20 nC to 90 nC [Figure 4F].

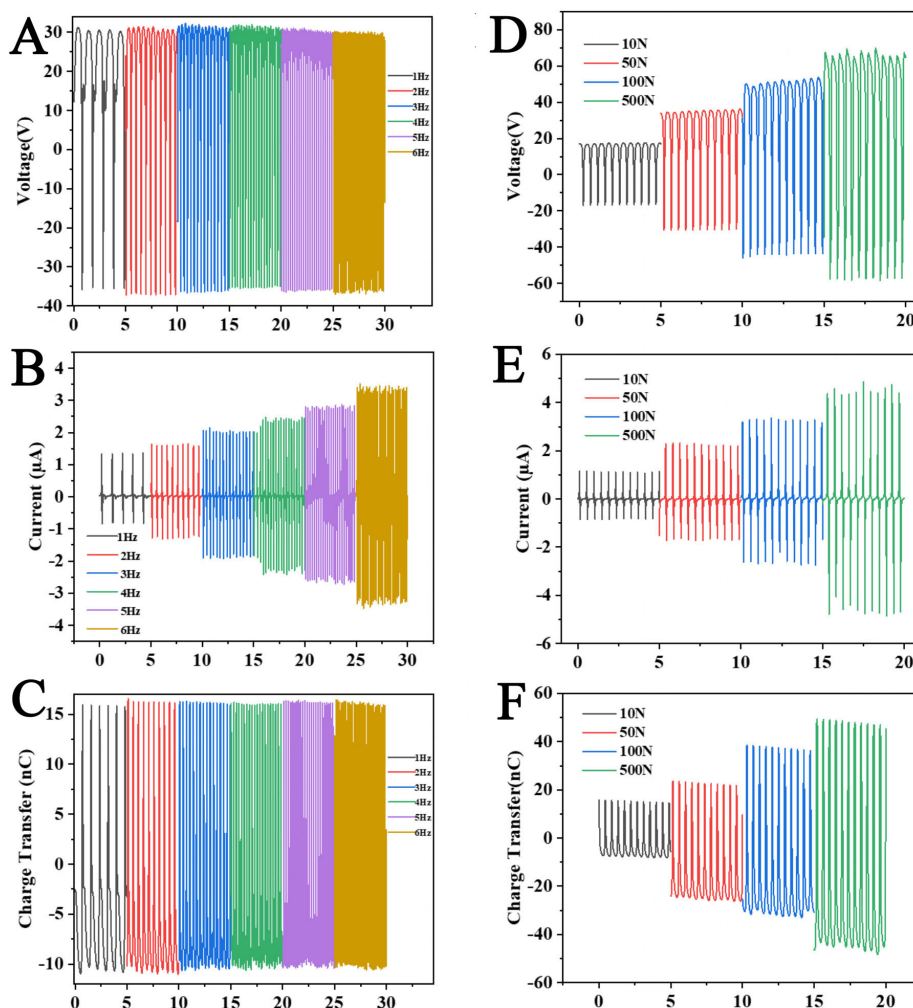


Figure 4. (A) Open circuit voltage; (B) Short circuit current; (C) Charge transfer at different frequencies from 1 Hz to 6 Hz; and (D) Open circuit voltage; (E) Short circuit current; (F) Charge transfer at different impact forces of 10 N, 50 N, 100 N, and 200 N, respectively.

As discussed above, when the frequency increased, the current of TENGs also increased while the charge and voltage changes were relatively small. This phenomenon could be mainly due to the capacitive nature of TENGs, where the electric charge stored on the TENG surface increased with the frequency but the voltage across the TENG remained relatively constant^[31]. As a result, the current generated by the TENG increased with frequency, leading to an enhancement in its electrical output. Moreover, the overall performance of the TENG also depended on other factors, such as material properties, surface roughness, operating conditions, and surrounding environment parameters including temperature, humidity, *etc.*

Applications

The output power density was evaluated by connecting with different external load resistances from 1 Ω to 500 $M\Omega$ at a working frequency of 3 Hz and force impact of 100 N. It can be noted that the current decreased as the resistance increased. Then, the instantaneous peak power density of TENGs can be calculated by $P=I^2R/S$, where P, I, R, and S denoted power density, output current, resistance, and size. The peak power density achieved maximum of 1.45 W/m^2 for Ag/g- C_3N_4 PDMS TENGs at the resistance of 20 $M\Omega$ [Figure 5A] and 1.5 W/m^2 for CNT/g- C_3N_4 PDMS TENGs at the resistance of 100 $M\Omega$ [Figure 5B],

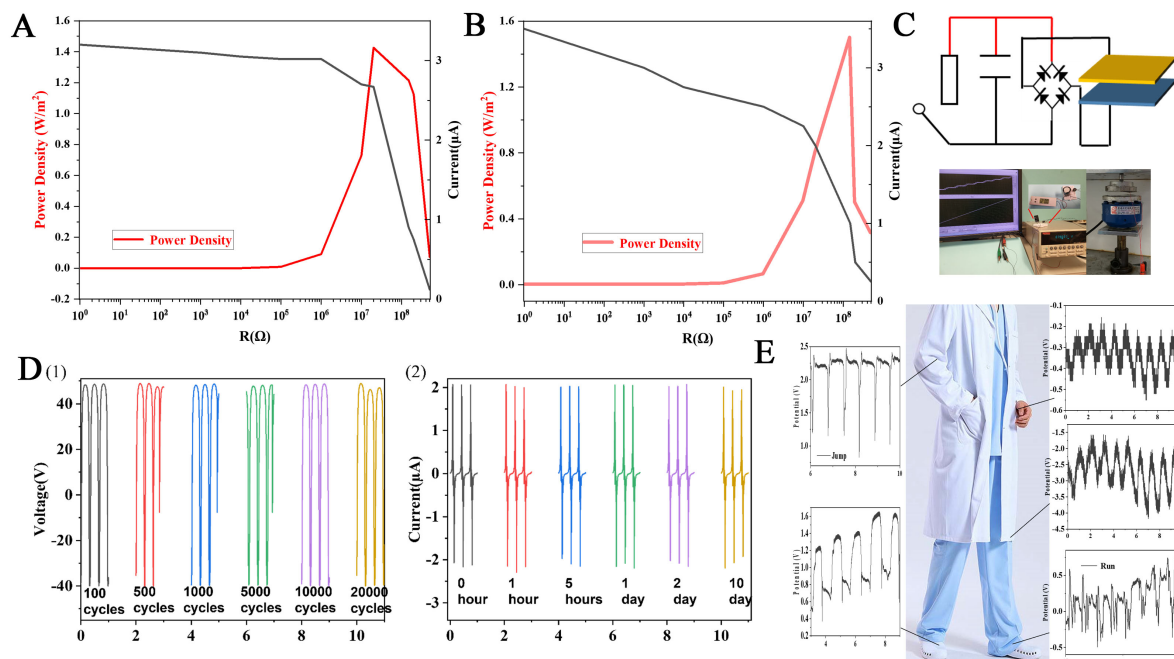


Figure 5. The instantaneous peak power density of (A) Ag/g- C_3N_4 PDMS TENG (B) CNT/g- C_3N_4 PDMS TENG at a series of external resistance loadings and the corresponding current output; (C) The equivalent circuit of charging capacitance and photographic demonstration; (D) Durability study for Ag/g- C_3N_4 PDMS TENG after (1) 100, 500, 1,000, 5,000, 10,000, and 20,000 cycles, respectively, as well as (2) 0 h, 1 h, 5 h, 1 day, 2 days, 10 days, respectively; (E) Applications of Ag/g- C_3N_4 PDMS TENG as self-powered wearable sensors. TENGs: Triboelectric nanogenerators; PDMS: polydimethylsiloxane; CNT: carbon nanotubes.

respectively. [Supplementary Table 1](#) in supporting information summarized TENGs with various dopants where our hybrid dopant/PDMS TENG showed better performance^[16]. To assess the potential of TENGs as energy sources, we investigated the charging capabilities of Ag/g- C_3N_4 PDMS TENG [Figure 5C], demonstrating the equivalent electrical circuit diagram of a self-powered system including a TENG as a power source, a capacitor as an energy storage unit, and a rectifier as an AC-to-DC converter. Typically, a smaller capacitance value results in a relatively higher charging speed. These findings suggested that TENGs can power small electronics such as calculators, watches or light emitting diodes (LEDs). By incorporating a TENG, capacitor, and rectifier into a self-powered system, the generated energy can effectively operate these devices. For instance, the TENG can simultaneously power over 40 LEDs [Supplementary Video 1]. The durability and storability were essential properties for devices, which would influence further applications. Ag/g- C_3N_4 PDMS TENG was experimented with continuous impact force up to 20,000 cycles and placed at room condition with temperature from 20 °C to 35 °C and humidity from 48% to 86% after immediately fabricated till ten days, which showed similar, stable, and steady results [Figure 5D], demonstrating relative high durability and stability little affected by the external environment. Based on its flexibility in real-world applications, TENG could be fabricated as a self-powered wearable sensor when attached onto human joints of the knee, wrist, and elbow, which had a rapid response to movement stimulus of 1.9 V, 0.3 V, and 1.1 V, respectively [Figure 5E and Supplementary Figure 3].

Subsequently, with a multichannel data acquisition system, the self-powered electric output via touch could recognize the tactile trajectory and detect the pressure distribution. A circular PDMS film was divided into eight equal segments with alternating conductive foil 1-4 to four channels for independent signal capture. Touching these sections activated a single electrode TENG, which could generate a voltage pulse (> 60 mV) in the corresponding channel while producing negligible signals in non-contacted channels [Figure 6A],

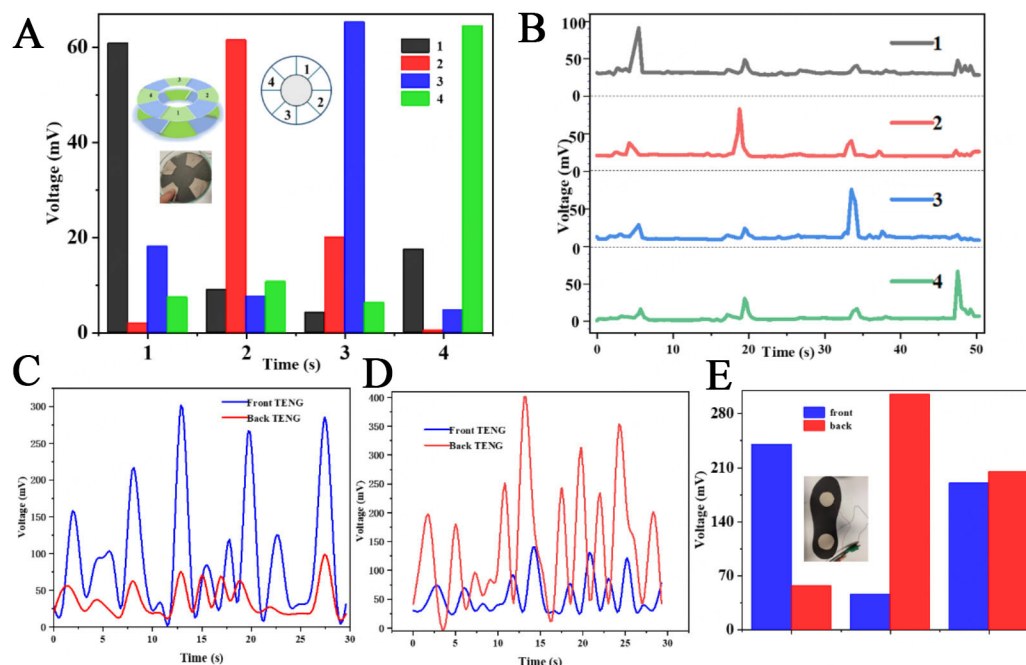


Figure 6. (A) Bar chart comparison of average sensing signals for a four-channel pressure sensing system, inset is the pattern illustration and real picture; (B) Sensing signal patterns by the sequence of pressing channels 1, 2, 3, and 4 in succession sequentially; (C) Signal pattern of the two-TENG insole while walking with the center of gravity at the front; (D) Signal pattern of the two-TENG insole while walking with the center of gravity at the back; (E) Bar chart comparison of average sensing signals while walking with center at the front, center at the back, and center at the middle, respectively, inset is the photo of the double-TENG insole. TENGs: Triboelectric nanogenerators.

enabling real-time touch localization through electronic signal tracking [Figure 6B]. Two round TENGs were also integrated into an insole at the front and back to monitor the center of gravity and analyze gait for posture correction using multichannel signal acquisition and processing. Voltage outputs, as depicted in Figure 6C, indicated a higher peak at the front TENG when weight was forward, and conversely, a higher rear TENG signal when weight shifted backward, as shown in Figure 6D. Balanced weight distribution resulted in nearly equal TENG signals, with average values and the insole's structure [Figure 6E]. Based on a digital multimeter with Bluetooth module and filter circuit module, the real-time signal generated by our TENG can be transferred wirelessly to personal mobile devices and displayed on software application functional interface [Supplementary Video 2].

EXPERIMENTAL

Materials

The silicone elastomer base and related curing agent for PDMS (SYLGARD® 184) were bought from Dow Chemical Company (USA). PDMS was fabricated by elastomer and curing agent with a ratio of 10:1. Stainless steel yarns (SSYs, Bekinox AISI 316L) were purchased from Bekaert (Belgium). CNF was purchased from 3M. CNTs, MXene, Ag, and AgO nanoparticles were from Dieckmann Company, and g-C₃N₄ powders were purchased from Xianfeng Nano Co. Ltd. All the materials were used as received without further purification.

Fabrication of g-C₃N₄ hybrid PDMS composite

Taking Ag nanoparticles and g-C₃N₄ powders as an example, two dopants were mixed at a certain ratio and added into the PDMS liquid homogeneously; after thorough ultrasonication for more than 12 h, 1 gram of

curing agent, and 9 grams of PDMS liquid were added into the mixture and stirred for 20 min. Subsequently, the mixture was transferred to a mold and spread evenly across the blade surface to avoid air bubbles into the mixture, and then kept in a desiccator under a vacuum oven at 80 °C for 12 h to form a self-standing film until it was completely cured, and finally stored in a clean dry environment to avoid touching the surface. After curing, the PDMS composite films were peeled off for further characterization and fabrication, with excess PDMS trimmed away using a scalpel. The curing time might vary depending on the thickness of the coating and the specific PDMS used, as well as the environmental index.

Assembly of PDMS TENG

PDMS was adhered to CNF to form the negative part and further cut into a square of 4 cm², and another piece of CNF was cut into the same size square as the counterpart acting as both tribomaterial and electrode, which was then contacted and separated. Finally, they adhered separately to two pieces of acrylic substrates for the triboelectric performance tests. The CNF electrodes were connected through copper wire and then to the electrometer to measure and collect signals of V_{oc} , I_{sc} and Q_{sc} .

Characterization and measurement

Fourier transforms infrared (FTIR) absorption spectra were recorded on a spectrometer (Spectrum 100, Perkin Elmer). The Raman spectra were acquired using a NomadicTM Raman 3-in-1 microscope with 532 nm lasers. The XRD patterns were recorded on an X-ray diffractometer (D8 Advance, Bruker) with Cu K α radiation to identify the crystalline phase. A Field Emission Scanning Electron Microscope (SEM, Tescan MIRA) was used to characterize the morphology and Energy Disperse Spectroscopy (EDS) data was acquired simultaneously. XPS spectra were investigated on an ESCALAB210 spectrometer. The output performance under impacting/releasing cycles was evaluated by utilizing a button/key durability life test machine (ZX-A03, Zhongxingda, Shenzhen) equipped with a self-configuring digital indicator (Interface 9860) to control the applied force at the precision of 0.1 N and range of 999 N. The output voltage signal was collected by Keysight DSO-X3014A oscilloscope and N2790A high voltage probe with 8 M Ω internal resistance. V_{oc} and I_{sc} were measured using an electrometer system Keithley 6514.

CONCLUSIONS

In summary, the hybrid dopants/PDMS composites were designed and prepared by embedding nanoparticles into the PDMS matrix, and experiments on ratio optimization with different hybrid dopants were carried out. Ag/g-C₃N₄ at the ratio of 3:1 at 1 wt % in PDMS composite manifested the best electrical properties with V_{oc} of 92 V, I_{sc} of 4.6 μ A, Q_{sc} of 49 nC, under 100 N and 3 Hz, and the optimized composite TENG reached output power density of 1.45 W/m². Similar to that of Ag/g-C₃N₄, CNT/g-C₃N₄, PDMS TENG presented the optimal mixture ratio at 1:1 to achieve the best electric performance of V_{oc} at 122 V, I_{sc} at 5.8 μ A, and Q_{sc} at 105 nC. Other groups of hybrid dopants including AgO/g-C₃N₄ and MXene/g-C₃N₄ were also evaluated. TENGs made from PDMS were flexible, resistant, and durable, which could be applied in wearable electronics and positioned at various joint parts of the human body. When connected to multichannel acquisition and signal processing devices, we designed a novel disc device that detected pressure at different locations and an insole that tracks the center of gravity of the gait to correct the walking posture. Our TENG could convert mechanical energy from human motion into electrical energy, providing energy sources and self-powered sensors for wearable devices. This work provided insights and a promising avenue for boosting the electrical output and practical applications of TENGs.

DECLARATIONS

Acknowledgments

The first author would like to acknowledge The Hong Kong Polytechnic University for providing postgraduate scholarship.

Authors' contributions

Substantial contributions to conceptualization, methodology, investigation, experimentation, data analysis and interpretation, and writing of the original draft: Xiao, Y.

Resources, methodology: Lu, J.

Supervision, writing review and editing: Xu, B.

Availability of data and materials

The data of the findings in this study are available from the corresponding author upon reasonable request.

Financial support and sponsorship

None.

Conflict of interest

All authors declared that there are no conflicts of interest.

Ethical approval and consent to participate

Not applicable.

Consent for publication

Not applicable.

Copyright

© The Author(s) 2025.

REFERENCES

1. Anlin, L. K.; Vijoy, K.; Pradeesh, K.; Thomas, S.; John, H.; Saji, K. Effects of metal nanoparticles on the performance of PDMS based triboelectric nanogenerators. *Phys. B. Condens. Matter.* **2022**, *639*, 413952. DOI
2. Zhang, H.; Zhang, X.; Qiu, C.; et al. Polyaniline/ZnO heterostructure-based ammonia sensor self-powered by electrospinning of PTFE-PVDF/MXene piezo-tribo hybrid nanogenerator. *Chem. Eng. J.* **2024**, *496*, 154226. DOI
3. Zhang, H.; Zhang, D.; Wang, D.; Xu, Z.; Yang, Y.; Zhang, B. Flexible single-electrode triboelectric nanogenerator with MWCNT/PDMS composite film for environmental energy harvesting and human motion monitoring. *Rare. Met.* **2022**, *41*, 3117-28. DOI
4. Shi, K.; Zou, H.; Sun, B.; Jiang, P.; He, J.; Huang, X. Dielectric modulated cellulose paper/PDMS-based triboelectric nanogenerators for wireless transmission and electropolymerization applications. *Adv. Funct. Mater.* **2020**, *30*, 1904536. DOI
5. Zhang, H.; Zhang, D.; Yang, Y.; et al. Eco-friendly triboelectric nanogenerator for self-powering stacked In₂O₃ nanosheets/PPy nanoparticles-based NO₂ gas sensor. *Nano. Energy.* **2024**, *128*, 109978. DOI
6. Xiao, Y.; Xu, B.; Bao, Q.; Lam, Y. Wearable triboelectric nanogenerators based on polyamide composites doped with 2D graphitic carbon nitride. *Polymers* **2022**, *14*, 3029. DOI PubMed PMC
7. Jiang, C.; Lai, C. L.; Xu, B.; So, M. Y.; Li, Z. Fabric-rebound triboelectric nanogenerators with loops and layered structures for energy harvesting and intelligent wireless monitoring of human motions. *Nano. Energy.* **2022**, *93*, 106807. DOI
8. Zhang, H.; Chen, X.; Liu, Y.; et al. PDMS film-based flexible pressure sensor array with surface protruding structure for human motion detection and wrist posture recognition. *ACS. Appl. Mater. Interfaces.* **2024**, *16*, 2554-63. DOI
9. Zhang, H.; Zhang, D.; Guan, J.; et al. A flexible wearable strain sensor for human-motion detection and a human-machine interface. *J. Mater. Chem. C.* **2022**, *10*, 15554-64. DOI
10. Sriphan, S.; Charoonsuk, T.; Maluangnont, T.; Vittayakorn, N. High-performance hybridized composited-based piezoelectric and triboelectric nanogenerators based on BaTiO₃/PDMS composite film modified with Ti_{0.8}O₂ nanosheets and silver nanopowders cofillers. *ACS. Appl. Energy. Mater.* **2019**, *2*, 3840-50. DOI
11. Zhu, Y.; Yang, B.; Liu, J.; et al. A flexible and biocompatible triboelectric nanogenerator with tunable internal resistance for powering wearable devices. *Sci. Rep.* **2016**, *6*, 22233. DOI PubMed PMC
12. Cheng, X.; Miao, L.; Song, Y.; et al. High efficiency power management and charge boosting strategy for a triboelectric nanogenerator. *Nano. Energy.* **2017**, *38*, 438-46. DOI
13. Zhang, H.; Zhang, D.; Mao, R.; et al. MoS₂-based charge trapping layer enabled triboelectric nanogenerator with assistance of CNN-GRU model for intelligent perception. *Nano. Energy.* **2024**, *127*, 109753. DOI
14. Li, Y.; Liu, C.; Zou, H.; et al. Integrated wearable smart sensor system for real-time multi-parameter respiration health monitoring. *Cell. Rep. Phys. Sci.* **2023**, *4*, 101191. DOI

15. Bayan, S.; Pal, S.; Ray, S. K. Interface engineered silver nanoparticles decorated g-C₃N₄ nanosheets for textile based triboelectric nanogenerators as wearable power sources. *Nano. Energy*. **2022**, *94*, 106928. DOI
16. Xiao, Y.; Li, Z.; Xu, B. Flexible triboelectric nanogenerators based on hydrogel/g-C₃N₄ composites for biomechanical energy harvesting and self-powered sensing. *ACS. Appl. Mater. Interfaces*. **2024**, *16*, 13674-84. DOI
17. Tang, J.; Er, C.; Kong, X. Y.; et al. Two-dimensional interface engineering of g-C₃N₄/g-C₃N₄ nano hybrid: synergy between isotype and p-n heterojunctions for highly efficient photocatalytic CO₂ reduction. *Chem. Eng. J.* **2023**, *466*, 143287. DOI
18. Li, H.; Jing, Y.; Ma, X.; et al. Construction of a well-dispersed Ag/graphene-like g-C₃N₄ photocatalyst and enhanced visible light photocatalytic activity. *RSC. Adv.* **2017**, *7*, 8688-93. DOI
19. Bokobza, L.; Bruneel, J.; Couzi, M. Raman spectra of carbon-based materials (from graphite to carbon black) and of some silicone composites. *C.* **2015**, *1*, 77-94. DOI
20. Hadjiivanov, K. I.; Panayotov, D. A.; Mihaylov, M. Y.; et al. Power of infrared and raman spectroscopies to characterize metal-organic frameworks and investigate their interaction with guest molecules. *Chem. Rev.* **2021**, *121*, 1286-424. DOI
21. Li, W.; Chen, F. Ultraviolet-visible absorption, Raman, vibration spectra of pure silver and Ag-Cu clusters: a density functional theory study. *Phys. B. Condens. Matter.* **2014**, *451*, 96-105. DOI
22. Ha, P. T. T.; Vu, X. H.; Dien, N. D.; et al. Ag nanoparticles on ZnO nanoplates as a hybrid SERS-active substrate for trace detection of methylene blue. *RSC. Adv.* **2022**, *12*, 7850-63. DOI PubMed PMC
23. Song, Y.; Gao, S.; Tian, J.; Zhang, H. Construction of Ag/g-C₃N₄ composites with uniform-sized Ag nanoparticles and the application for sulfisoxazole degradation in the presence of visible radiation. *J. Environ. Chem. Eng.* **2020**, *8*, 104390. DOI
24. Xiao, Y. Design, fabrication, and application study of droplet tube based triboelectric nanogenerators. *Tribol. Ind.* **2023**, *45*, 699-709. DOI
25. Niu, S.; Wang, Z. L. Theoretical systems of triboelectric nanogenerators. *Nano. Energy*. **2015**, *14*, 161-92. DOI
26. Bulathsinghala, R.; Ravichandran, A.; Zhao, H.; Ding, W.; Dharmasena, R. The intrinsic impact of dielectric constant on output generation of triboelectric nanogenerators. *Nano. Energy*. **2024**, *123*, 109383. DOI
27. Liu, Z.; Muhammad, M.; Cheng, L.; Xie, E.; Han, W. Improved output performance of triboelectric nanogenerators based on polydimethylsiloxane composites by the capacitive effect of embedded carbon nanotubes. *Appl. Phys. Lett.* **2020**, *117*, 143903. DOI
28. Wang, D.; Bao, Y.; Zha, J. W.; Zhao, J.; Dang, Z. M.; Hu, G. H. Improved dielectric properties of nanocomposites based on poly(vinylidene fluoride) and poly(vinyl alcohol)-functionalized graphene. *ACS. Appl. Mater. Interfaces*. **2012**, *4*, 6273-9. DOI
29. Saini, P.; Choudhary, V.; Singh, B.; Mathur, R.; Dhawan, S. Polyaniline-MWCNT nanocomposites for microwave absorption and EMI shielding. *Mater. Chem. Phys.* **2009**, *113*, 919-26. DOI
30. Suo, X.; Li, B.; Ji, H.; et al. Dielectric layer doping for enhanced triboelectric nanogenerators. *Nano. Energy*. **2023**, *114*, 108651. DOI
31. Xiao, Y.; Li, Z.; Tan, D.; Carsten, G.; Xu, B. Triboelectric nanogenerators based on transition metal carbo-chalcogenide (Nb₂S₂C and Ta₂S₂C) for energy harvesting and self-powered sensing. *Adv. Sci.* **2024**, *11*, e2409619. DOI